Graphene/SiC(0001) interface structures induced by Si intercalation and their influence on electronic properties of graphene

Anton Visikovskiy,[1,*] Shin-ichi Kimoto,[1] Takashi Kajiwara,[1] Masamichi Yoshimura,[2] Takushi Iimori,[3] Fumio Komori,[3] and Satoru Tanaka[1]

[1]*Department of Applied Quantum Physics and Nuclear Engineering, Kyushu University, Fukuoka 819-0395, Japan*

[2]*Toyota Technological Institute, Nagoya 468-8511, Japan*

[3]*Institute of Solid State Physics, University of Tokyo, Kashiwa 277-8581, Japan*

(Received 8 April 2016; revised manuscript received 5 October 2016; published 19 December 2016)

Epitaxial graphene growth on SiC surfaces is considered advantageous in terms of device application. However, the first graphitic layer on SiC transforms to a buffer layer because of strong coupling with the substrate. The properties of several subsequent layers are also significantly degraded. One method to decouple graphene from the substrate is Si intercalation. In the present work, we report observation and analysis of interface structures formed by Si intercalation in between the graphene layer and the SiC(0001) surface depending on Si coverage and influence of these interfaces on graphene electronic structure by means of low-energy electron diffraction (LEED), scanning tunneling microscopy (STM), angle-resolved photoemission spectroscopy (ARPES), and theoretical first-principles calculations. The STM appearance of observed periodic interface structures strongly resembles previously known Si-rich phases on the SiC(0001) surface. Based on the observed range of interface structures we discuss the mechanism of graphene layer decoupling and differences in stability of the Si-rich phases on clean SiC(0001) and in the graphene/SiC(0001) interface region. We also discuss a possibility to tune graphene electronic properties by interface engineering.

DOI: 10.1103/PhysRevB.94.245421

I. INTRODUCTION

For some time now, graphene is speculated to be the material for post-Si era electronic devices, thanks to its extremely high carrier mobility and their extremely long (micrometer order) mean-free path [1–3]. Technological applications demand large-scale, high-quality, cheap, and simple ways to produce graphene sheets. The mechanical exfoliation methods and chemical synthesis do not meet these requirements. Chemical vapor deposition (CVD) on metal surfaces is an appropriate technique, but to be used in electronic devices, graphene has to be transferred from metal substrates onto insulating or semiconducting ones—often a complicated procedure accompanied with defects creation. One of the most promising methods of graphene synthesis for device application is epitaxial growth on SiC substrates [4]. SiC is a wide band-gap semiconductor material commonly used in high-temperature and high-power electronic devices, so there is no need for graphene transfer. Graphene based devices can be formed directly on the SiC substrate, which significantly simplifies the production and reduces the probability of defects formation. The growth process includes surface thermal decomposition with Si sublimation from the sample surface in ultrahigh vacuum (UHV) or argon atmosphere [5]. The growth dynamics of graphene on C-terminated SiC(000$\bar{1}$) and Si-terminated SiC(0001) surfaces significantly differs. The latter surface offers significantly lower growth rates and, therefore, higher control over the number and uniformity of graphene layers. Plus, graphene layers on SiC(0001) are orientationally aligned with the substrate (30° rotation of graphene lattice with respect to the SiC) [6], making it easy to build crystal orientation sensitive nanostructures. The main problem with epitaxial graphene growth on SiC substrates is a high density of reactive dangling bonds on the surface, which hybridize with electronic states of graphene and significantly alter its electronic structure. It is commonly accepted that the first carbon layer on the SiC(0001) surface has graphenelike atomic structure [7–9] but lacks characteristic graphene's π and π^*-bands completely due to the substrate influence. This layer exhibits $(6\sqrt{3} \times 6\sqrt{3})$R30° (further referred to as $6\sqrt{3}$) periodic structure with respect to the SiC(0001) substrate and is called a buffer layer or zeroth layer graphene. The following layers grown on top of the buffer layer retain graphene's specific band dispersion, but still the substrate influence appears to degrade carriers mobility significantly compared to the free-standing graphene samples [3,9,10]. An effective approach to this problem is to decouple graphene from the substrate influence by means of atomic intercalation and saturation of the Si dangling bonds at the graphene/SiC(0001) interface. Widely used for this purpose hydrogen intercalation allows effective buffer layer decoupling and restoration of characteristic graphene's electronic bands in so-called quasi-free-standing graphene layers [11,12]. There have been reports on the possibility of other elements (Li [13], Au [14], Ge [15,16], Si [17–22], O [23,24], Cl [25]) intercalation resulting in graphene's decoupling (here and following the term 'decoupling' is used to define the process of restoration of characteristic π and π^* bands of graphene with or without band gap opening, rather than complete removal of interaction between graphene and substrate) and even modification of its electronic structure. Recently, Si intercalation attracted attention owing to its compatibility with present semiconductor technology and nondestructive nature of penetration through the graphene sheet [20,21]. It has been shown that Si intercalation results in the buffer layer decoupling from the substrate and restores characteristic Dirac conelike electronic structure [22,26].

*Corresponding author: anton_v@nucl.kyushu-u.ac.jp

Although the fact of electronic decoupling of graphene from the substrate is important, it is more important to know how graphene's electronic properties are affected by the interface structure and whether it is possible to tune these properties using interface interaction. The urge for such graphene electronic structure modification comes from the essentially gapless nature of this material. Because of zero band gap, the current in the devices with channels made of graphene cannot be 'switched off' and, therefore, perfect graphene is not suitable for application in modern devices with traditional switching logic. The band gap in the electronic structure of graphene can be created in several ways. For example, one can employ the quantum confinement effect and edge states of narrow graphene nanoribbons (GNRs) [27,28], or apply bias to bilayer or trilayer graphene [29,30], or use strained graphene [31]. An alternative interesting option is to apply periodic potential to the graphene layer [32–34]. In certain cases, this potential may create perturbation in the interaction of hexagonally arranged sp^2 bonded C atoms and break the intrinsic sublattice symmetry resulting in band-gap opening [35]. Such periodic potential is actually realized by the graphene/substrate interface layer. Therefore, the atomic structure of the interface and its influence on graphene's electronic properties are extremely important to know, as it may serve a key role in graphene application.

In the present paper we would like to address these two questions: the atomic structure of interfaces formed by Si atoms intercalation into a graphene/SiC region and the prospectives to use such structures for graphene's electronic properties modification. Although previous reports stated low-energy electron diffraction (LEED) observations of (3×3) periodicity in the Si intercalated system [19], no detailed study of this or other interfaces has been carried out so far. Here, we show our results obtained by scanning tunneling microscopy (STM), angle-resolved photoemission (ARPES), LEED and first principles theoretical calculations on atomic structure, and electronic properties of interfaces created by Si intercalation. We have found that higher Si coverage interface structures are similar to those formed by Si deposition on clean SiC(0001) without the presence of graphene. The stability of these reconstructions, however, appears to be quite different with the presence of graphene overlayer. There were no well ordered lower coverage structures observed. We have suggested a descriptive principal model of graphene decoupling during the intercalation process.

II. EXPERIMENTAL DETAILS

In the present study we used vicinal 6H-SiC(0001) samples with a 4°-off axis miscut angle towards $[1\bar{1}00]$. The choice of vicinal over on-axis samples is justified (1) by the abundance of the samples in stock in our laboratory (we mainly specialized on vicinal SiC surfaces), (2) by increased efficiency and uniformity of Si intercalation. As was shown experimentally [18] and by calculations [21] in previous works, Si intercalation occurs only through atomic defects in a graphitic layer, as the perfect graphene is impenetrable for Si atoms. The graphene layer covers steps and facets of the SiC surface in a carpetlike manner, but eventually, owing to higher reactivity and morphological curvature, the defect density in the graphene sheet is larger near steps and facets than on flat terrace areas. So, the vicinal surface would be advantageous for efficient and uniform Si intercalation.

The samples were etched in an H_2 atmosphere at 1660 K for 30 min to produce a regular surface consisting of (0001) terraces and $(1\bar{1}0n)$ facets. The samples were then transferred to a UHV chamber (base pressure $<10^{-9}$ Pa), flashed at 1520 K and cleaned by repeating annealing in Si flux at 1320 K until sharp $(\sqrt{3} \times \sqrt{3})$R30° (further referred to as $\sqrt{3}$) pattern of clean SiC(0001) terminated with Si adatoms was observed by LEED. Graphene's buffer layer has been grown by surface decomposition in UHV conditions by annealing the sample at 1550 ∼ 1690 K for 30 min. The formation of the buffer layer has been monitored by means of reflection high-energy electron diffraction (RHEED), LEED, which showed a sharp $6\sqrt{3}$ pattern, and confirmed by STM.

Si intercalation has been carried out by deposition of Si atoms from heated to a ∼1300 K Si wafer onto the sample kept at elevated temperature (970 ∼ 1120 K) or on the sample kept at room temperature (RT) with subsequent annealing at the same temperatures for several minutes. Both methods give similar results. The amount of intercalated Si was controlled by the deposition time. The samples were then studied *in situ* by LEED, STM (Omicron VT-STM, chemically etched tungsten tips), and ARPES (SPECS UVS300, 3 mmϕ surface area detection, sample at 130 K, He Iα UV source) and *ex situ* Raman spectroscopy and x-ray photoemission spectroscopy (XPS).

III. RESULTS

The evolution of LEED patterns with Si deposition is shown in Fig. 1. The initial surface shows sharp and clear characteristic $6\sqrt{3}$ spots [Fig. 1(a)]. There are some traces of so-called "5 × 5" structure. This latter reconstruction is often observed together with $6\sqrt{3}$. Its STM appearance shows clusters of protrusions which are arranged locally in $\sqrt{3}$ order with respect to SiC-(1×1). The clusters are not of regular shape, however, they exhibit average (5×5) periodic arrangement. The origin of this phase is still debatable: Some refer to it as graphene's moiré pattern locally distorted from its usual $6\sqrt{3}$ substrate period matching, while others seem to support the hypothesis that this phase originates from islands of Si adatoms retaining $\sqrt{3}$ local configuration under the graphene layer. While the structure of this phase is out of the scope of the present paper, we have to note that the initial "5 × 5" phase survives throughout the whole Si intercalation process, as indicated by the presence of "5 × 5" diffraction spots in all the LEED patterns and STM images (see Fig. 2). There is even some increase in the intensity of "5 × 5" spots as well as observed coverage of "5 × 5" patches in STM images with increase of the amount of intercalated Si, which may support the latter, Si adatom origin hypothesis, although there is not enough reproducible data to justify these conclusions.

With the increase of Si coverage the original $6\sqrt{3}$ diffraction pattern appears to fade away with significant rise of background intensity. After that (in ∼40 min deposition time, depending on the Si source), some additional spots appear manifesting the formation of rather complicated reconstruction [Fig. 1(b)]. The exact periodic structure could not be

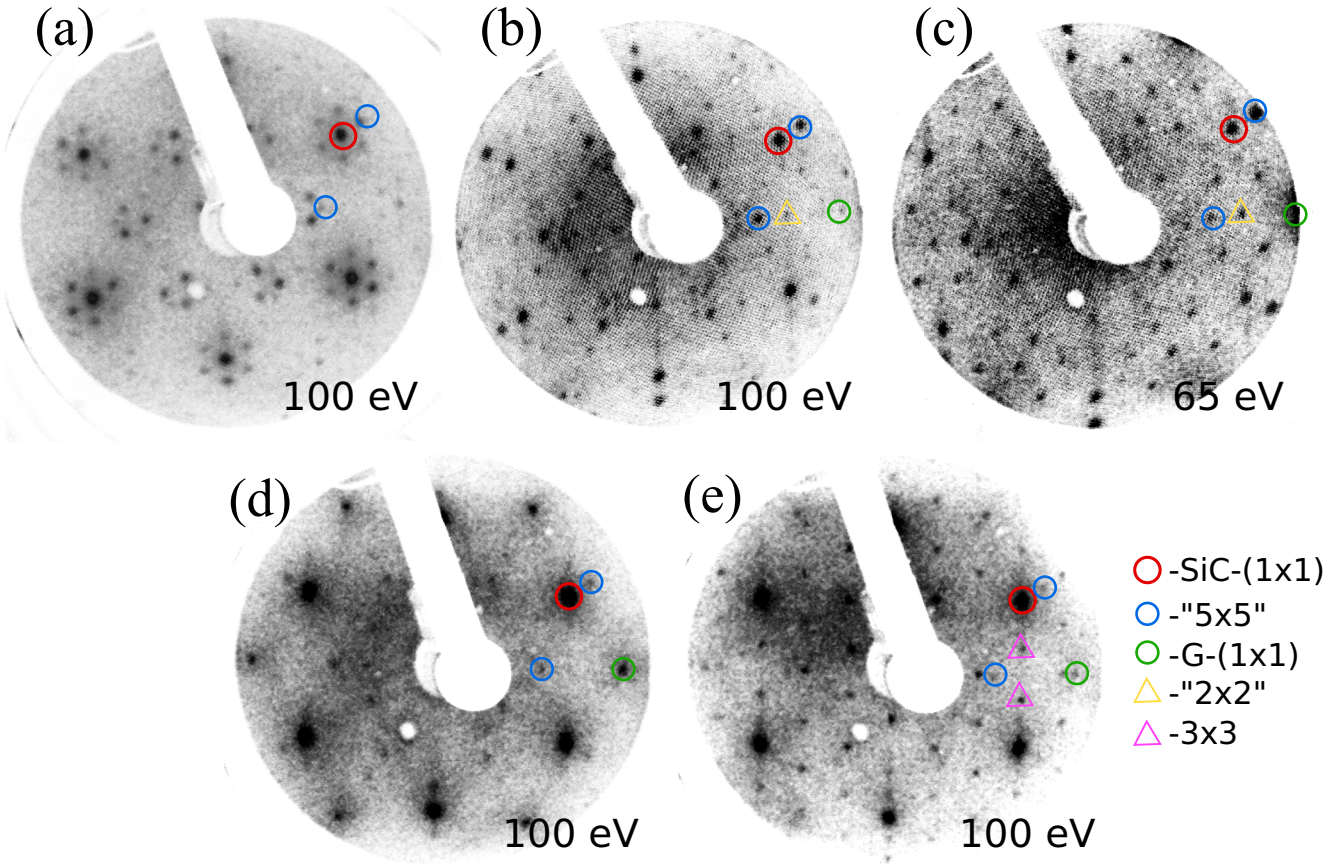

FIG. 1. Evolution of surface structures as observed by LEED: (a) the initial $6\sqrt{3}$ structure, (b) intermediate amount of intercalated Si (40 min deposition), the structure is denoted as "2 × 2", (c) the same structure pattern but acquired at lower electron incident energy revealing half-order spots more clearly, (d) the LEED pattern exhibiting high background (60 min deposition), (e) (3 × 3) LEED pattern obtained by Si intercalation (70–90 min Si deposition).

determined owing to rather low intensity of the additional spots. It is clear, however, that half-order spots appear in the LEED pattern, which are especially apparent at lower incident electron energy, as shown in Fig. 1(c). So, we denote this phase as "2 × 2". The further Si coverage increase results in disappearing of the additional spots corresponding to this superstructure. The next phase formed at the interface after ∼60 min of total Si deposition time and, despite the good periodicity (see STM results below), surprisingly results in rather broad spots with high background intensity [Fig. 1(d)]. Variation of incident beam energy reveals the existence of some additional spots, but with very low spot/background intensity ratio. Decoupling of the buffer layer from the substrate and converting it to the first graphene layer are obvious from these patterns by the increased (compared with $6\sqrt{3}$) intensity of graphene (1 × 1) spots. Finally, upon intercalation of enough Si (70 ∼ 90 min deposition time), a (3 × 3) structure appears [Fig. 1(e)]. Again, the decoupled graphene layer manifests itself by existence of graphene's diffraction pattern. Also, some minor "5 × 5" spots are still visible together with some faint high-order spots which correspond, probably, to the coexistence of previously mentioned structures or a moiré pattern between the graphene and interface layer.

Next, we discuss the STM appearance of the intercalated interfaces. Figure 2(a) shows the initial surface of the sample covered by buffer layer $6\sqrt{3}$. There are also patches of "5 × 5" reconstruction, which appears as irregular islands of protrusions (with local $\sqrt{3}$ arrangement) [Fig. 2(b)]. Upon Si intercalation (20 ∼ 40 min deposition time), large regions of disordered structure start to appear on the surface [Figs. 2(c) and 2(d)]. Finally, the ordered reconstruction is developed, having hexagonal protrusion arrangement [so, referred to further as 'hex' structure shown in Figs. 2(e) and 2(f)]. As one may see from the detailed STM image [Fig. 2(f)], each structural unit of this phase consists of a large central triangular shaped protrusion surrounded by six smaller ones. Some of the central protrusions are in a 'doped' state, appearing significantly brighter than others. From the STM appearance, this structure has a hexagonal unit cell (shown in yellow in the STM image) with a lattice size of ∼2 nm and ∼8° rotated with respect to the SiC lattice. This would correspond to [(7,1),(−1,6)] periodicity. The hexagonal arrays of the smaller protrusions, however, have the arrangement close to those of (2 × 2) of the SiC surface. Thus, this structure may produce half-order reflexes observed in the "2 × 2" LEED pattern [Fig. 1(c)]. It is interesting to note that very similar reconstruction has been observed previously for Si deposition on a clean SiC(0001) surface (see Ref. [36]).

The next structure observed for a larger amount of intercalated Si (∼60 min deposition time) is shown in

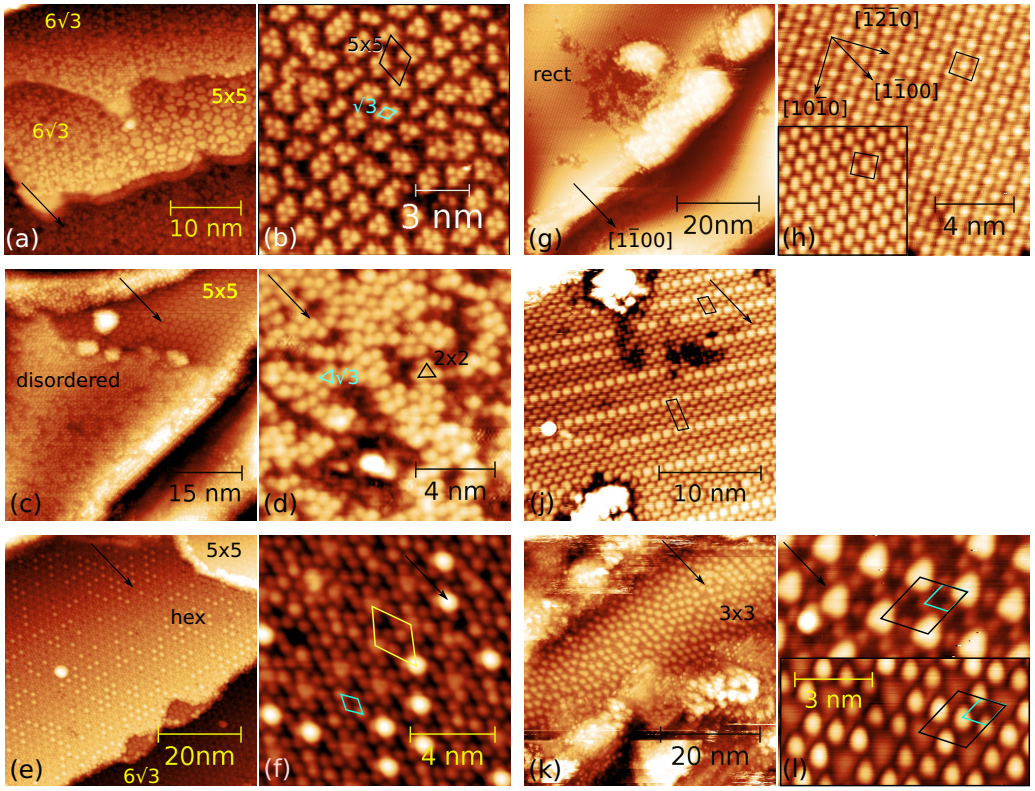

FIG. 2. Evolution of the surface structure as observed by STM (the arrow on all images denote [1$\bar{1}$00] direction): (a) the initial $6\sqrt{3}$ structure, "5 × 5" patches are also observed; (b) enlarged view of "5 × 5" structure, the 5 × 5 quasiperiodic cell is shown by black rhombus, while local $\sqrt{3} \times \sqrt{3}$ arrangement by cyan (c), (d) large scale and magnified STM images of disordered areas (20 ∼ 40 min Si deposition time), note on the enlarged image the existence of both $\sqrt{3}$ and 2 × 2 local arrangements shown in cyan and black, respectively; (e) hexagonal-like structure denoted as "2 × 2" [corresponding LEED pattern is in Fig. 1(b), 1(c) for ∼40 min Si deposition time], (f) the hexagonal unit cell (yellow) with $a \approx 2$ nm and ∼8° rotation with respect to the SiC lattice, the individual protrusions show periodicity (cyan cell) close to (2 × 2) of SiC, (g) the rectangular-like structure [corresponding LEED pattern is in Fig. 1(d), ∼60 min deposition time], (h) magnified image of rectangular-like structure, which corresponds to $(2\sqrt{3} \times 4)$; (j) domain boundary lines observed in rectangular-like $(2\sqrt{3} \times 4)$ structure; (k) (3 × 3) interface obtained by Si intercalation (∼90 min deposition time), note high degree of disorder in bright protrusion locations observed in filled-state image, (l) (3 × 3) reconstruction (cyan unit cell), note that in contrast to LEED pattern [Fig. 1(e)], STM shows strong modulations with double periodicity (black unit cell), corresponding to actual (6 × 6) cell.

Figs. 2(g)–2(j). This one is represented by the rectangularlike array of protrusions (hence, denoted as 'rect'). The close examination [Fig. 2(h)] shows that there are pairs of brighter and dimmer alternating protrusions in rows. The protrusions pairlike appearance is amplified in the empty-state STM image, where each pair is imagined as a single oval-shaped protrusion [as shown in the inset in Fig. 2(h)]. The region shown in Fig. 2(g) is rather uniform, which is not always the case. In some places, the surface is crossed by bright lines of domain boundaries between adjacent rectangular structures with the lateral shift of half-unit cell along protrusion rows [Fig. 2(j)]. The preferential distance between these boundaries leads to extended periodicity in this direction. However, different locations on the surface show a slightly different period between boundary lines [see different unit cells in Fig. 2(j)]. The periodicity of the surface in the region free of domain boundaries is $(2\sqrt{3} \times 4)$. In other places it varies. It is rather unusual that this interface does not produce a decent LEED pattern [see corresponding LEED in Fig. 1(d)] considering the high level of ordering. Interestingly again, a similar structure has been previously observed in the case of Si deposition on clean SiC(0001) in Refs. [36,37], although in those reports the periodicity was determined with the account of regular periodic domain boundaries structure as $(2\sqrt{3} \times 2\sqrt{13})$.

Finally, the STM image corresponding to (3 × 3) diffraction pattern is shown in Figs. 2(k) and 2(l). The filled-state STM image does not show (3 × 3) periodicity right away. The surface appears to consist of a (3 × 3) mesh of small and dim protrusions [cyan unit cell in Fig. 2(l)] overlayed with large bright triangular-shaped protrusions of "6 × 6" period (black unit cell) in the most cases and showing some degree of disorder in other places. The empty-state image, shown in the lower part of Fig. 2(l), has a more close resemblance to the usual (3 × 3) appearance of the Si-rich SiC(0001) surface. The brightness variation of the protrusions repeats the filled-state "6 × 6" pattern in the inverted manner—bright protrusions in the filled-state image correspond to dimmer ones in the empty state image, pointing out that this has to be an electronic structure effect rather than a topographic feature.

It is worth noting also, that in contrast to the $6\sqrt{3}$ structure, all Si intercalated structures clearly show a graphene overlayer in the STM image at low-bias condition (see Fig. 3),

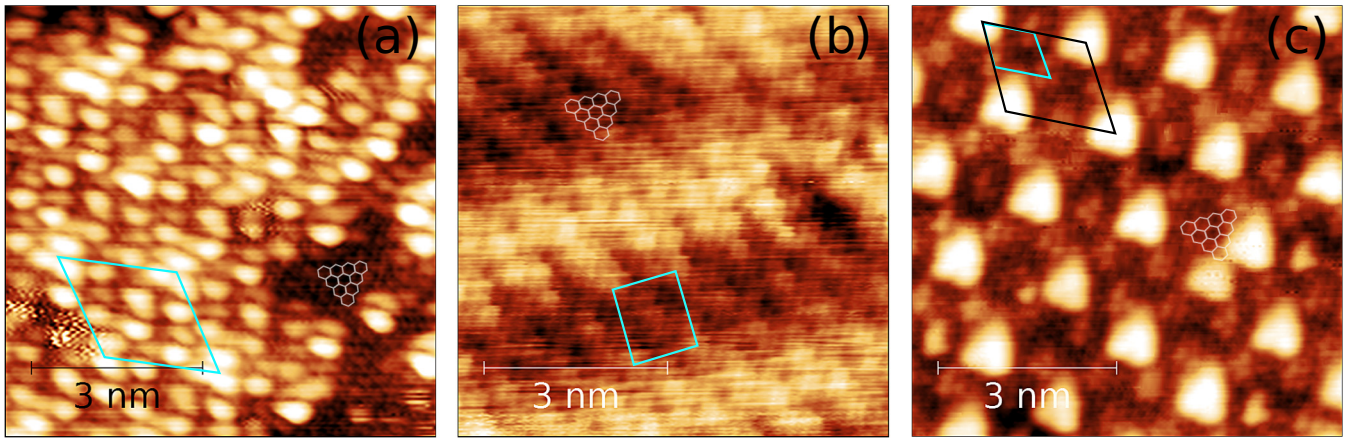

FIG. 3. Low-bias STM images of Si-intercalated interface structures: (a) hexagonal "2 × 2" interface, (b) rectangular ($2\sqrt{3} \times 4$), domain boundaries look like bright diagonal stripes, (c) (3×3) interface. One may clearly see the graphene overlayer lattice on top of the mentioned structures.

indicating that these are indeed interface structures formed under graphene layer, and graphene is partially decoupled from the substrate, so it could be imagined by STM. The decoupling of the graphene layer is also evident from *ex situ* Raman spectroscopy showing clear characteristic graphene G, D, and G′ bands (not shown here) and by the appearance of clear Dirac cone dispersion due to single graphene layer in ARPES data as shown in Figs. 4(b) and 4(c). Characteristic graphene bands appear for all substantial coverages of intercalated Si with noticeable *n*-type doping, as seen from the Dirac point location below the Fermi level: ∼−0.2 eV for the lower coverage 'hex' structure and ∼−0.3 eV for the (3×3) interface. In the latter case, some broadening of electron dispersion is observed, which can be explained by additive contribution from different structures, because, at least in STM experiments, we could not obtain a full (3×3) interface phase to cover the entire observable area without inclusion of lower coverage patches.

From the rather evident resemblance of STM appearances of Si intercalated structures to those observed previously in cases of Si deposition on clean SiC(0001), one may draw a conclusion that Si just forms typical reconstructions on SiC(0001), so the atomic structure of the interface layers, in terms of general atomic arrangement, are similar to those of Si-rich superstructures on clean SiC(0001). Beside STM appearances, another fact to support this hypothesis, at least for well known (3×3)-Si phase on clean SiC(0001), is normalized core-level x-ray photoemission data of the Si 2*p* peak shown in Fig. 4(d). As one can see, the peak position and shape of the graphene/SiC interface structure exactly reproduces the peak for Si-rich clean SiC(0001)-(3×3) structure despite complex, several component composition. The present observations would not mean that the graphene layer is completely ignored during interface structure formation. Let us point out some differences. There are several Si-rich phases reported to exist on clean SiC(0001). They are, in the order of increasing Si coverage, ($\sqrt{3} \times \sqrt{3}$), (4×4), "2 × 2", ($2\sqrt{3} \times 2\sqrt{13}$), ($3 \times 3$) [36,38]. The $\sqrt{3}$ and (3×3) phases, being the most stable, are observed in a relatively broad range of Si coverages. The (4×4), "2 × 2", ($2\sqrt{3} \times 2\sqrt{13}$) reconstructions were reported only for quite limited formation conditions and mostly appear in the form of small patches, primarily near step edges, being surrounded by more stable reconstructions [36,37]. In the case of the graphene overlayer, however, only three of these phases with higher Si coverage were observed. There were no $\sqrt{3}$ or (4×4) interface structures. The "5 × 5" reconstruction with

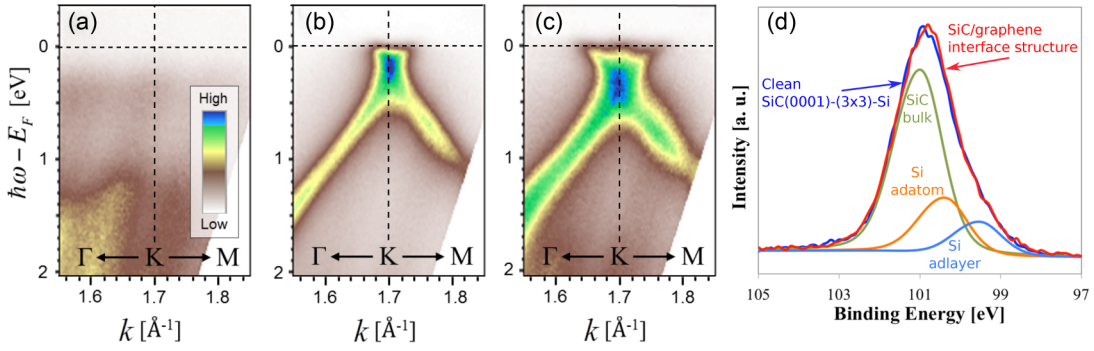

FIG. 4. ARPES data showing the band structure in the vicinity of graphene's Brillouin zone *K* point. (a) Before Si deposition, (b) after 90 min of Si deposition, corresponding to rectangularlike structure, (c) after 240 min of Si deposition, corresponding to (3×3) interface structure. (d) Normalized XPS data of Si 2*p* peak, showing close resemblance in position and peak shape between clean SiC(1000)-(3×3)-Si phase and (3×3) SiC/graphene interface structure.

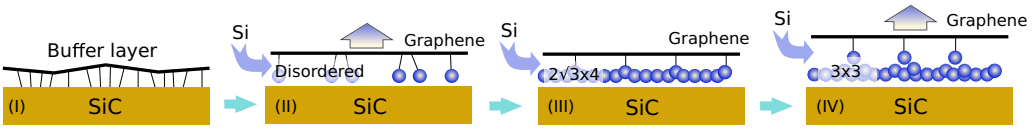

FIG. 5. The qualitative model of Si intercalation into graphene/SiC(0001) interface. (I),(II) The buffer layer is detached from the substrate and the new graphene layer is lifted to accommodate Si adatoms. (II),(III) Si concentration at the interface is increased up to around one monolayer. (III),(IV) To accommodate additional Si, the graphene layer has to be detached and lifted again.

local $\sqrt{3}$ protrusions arrangement observed in vast amounts on the surface has been, by the most part, formed before Si intercalation. The analysis of the disordered interface structure [Fig. 2(d)] reveals that most of the protrusions are grouped by two or three and has local separations characteristic to the $\sqrt{3}$ and 2×2 structure (real space distance measurements, plus 2D Fourier transformation of STM image analysis), though these groups positions are randomized with respect to each other. Thus, the disordered interface may to some extent be the analog of Si-rich $\sqrt{3}$ reconstruction on clean SiC(0001). Based on these observations we may suggest a model of graphene decoupling process and interface formation (Fig. 5). Initially Si atoms intercalate a buffer layer through defect sites. The number of defect sites is limited, thus there are only a minor amount of interface entry points. The graphene buffer layer is strongly bonded to the substrate Si atoms (up to $1/3$ of C atoms in the buffer layer according to Ref. [39], meaning almost all the surface Si are participating). This makes it extremely difficult for intercalated Si to migrate from the entry point further into the interface region, as it has to break several C-Si bonds to detach and lift the buffer layer locally [Fig. 5(II)]. Due to confined space available at the interface the kinetic barriers for Si migration also should be higher. So, intercalated Si adatoms tend to move much slower through higher barriers and there is no enough temperature and time to arrange them in the perfect long range $\sqrt{3}$ pattern. The position of Si adatoms at the interface is stabilized not only by interaction through the substrate as in the case of clean SiC(0001), but also by bonding with C atoms of the graphene layer. According to calculations, the on-top site location of the graphene C atom with respect to Si adatoms is $\sim$0.5 eV more favorable than the hollow site, meaning that Si adatoms will mostly concentrate at sites with C of the graphene overlayer directly on top or nearby. As the position of C atoms is not well correlated with the position of T_4 sites on the SiC surface (due to lattice mismatch), the resultant optimal adatom positions do not necessarily have to be in $\sqrt{3}$ mesh. These are probably the reasons for disordered interface formation. Once the buffer layer is partially detached by Si adatoms the penetration and diffusion of Si atoms at the interface becomes easier. This leads to rapid conversion to more ordered interface structures with higher Si coverage such as 'hex' and 'rect' ones [Fig. 5(III)]. Although the structures of corresponding phases on clean SiC(0001) are unknown, judging by their smaller relative coverage and the structure of known high coverage (3×3) reconstruction (Si adlayer +Si adatoms), one may safely imply that these phases consist of a complex mesh of Si atoms located in nearly the same plane (Si adlayer only). So, once the bonding between buffer layer and SiC surface is broken and graphene is detached by initial intercalation, the formation of the Si adlayer at the interface becomes much easier. While on the clean SiC(0001) surface these superstructures might lack stability compared to $\sqrt{3}$ and (3×3) due to the amount of unsaturated dangling bonds or geometrical distortions, at the interface the stability might be increased significantly by the coupling with the graphene layer (although a much weaker one than that between buffer layer and bulk terminated SiC due to a much lower density of dangling bonds) and spatial confinement. To build (3×3) reconstruction at the interface additional space is required to accommodate Si adatoms over the Si adlayer. This creates an additional energy barrier for (3×3) formation required for braking graphene—Si adlayer bonds and lifting graphene layer [Fig. 5(IV)]. Thus, the 'rect' structure appears to be most wide spread (it covers almost the entire surface, as observed by STM) at this amount of intercalated Si, as it is the highest coverage stable phase still having Si atoms roughly in the same plane. These observations show that although the variety of interface Si reconstructions looks similar to those on clean SiC(0001), there are some substantial differences due to the existence of the graphene overlayer.

The atomic structures of Si-induced "2×2" and rectangularlike $(2\sqrt{3} \times 4)$ phases on SiC(0001) are still unknown and under investigation. However, the structure of the SiC(0001)-(3×3)-Si phase is relatively well established using various methods [40,41]. So, we can use it as a model for (3×3) interface reconstruction between the SiC surface and graphene layer and test it out in theoretical calculations. The (3×3)-Si phase consists of Si adlayer, Si trimers, and Si adatom. The peculiar feature of this model is the high degree of Si bond saturation. Of 13 additional Si atoms in the unit cell, only the single Si adatom has a single dangling bond, which can be used to interact with carbon atoms of the on-top graphene layer. Such sparse dangling bonds act as a periodic and very localized (in contrast to slowly changing) potential on graphene's electronic structure. This topic has been addressed previously using *ab initio* calculations. It has been shown that graphene's band structure is extremely sensitive to the actual periodicity of such perturbation, and the condition of the band gap opening depending on the periodicity of the perturbing potential has been established [33,34]. Our density functional theory (DFT) calculations (the in-depth detailed analysis is out of the scope of the present paper and will be published elsewhere) is in general agreement with these studies, but also provide some additional insight in band structure dependence on the local structure of periodic defects and its periodicity. Here we note that there would be a notable difference between an Si dangling bond located directly under the carbon atom (on-top site), in the hollow, or on the bridge site of the graphene lattice. For example, our calculations show that the graphene unit cell containing a single on-top interaction site would produce no gap between π and π^* bands for hexagonal unit cell sizes that are multiples of the $\sqrt{3}$ cell of the graphene lattice,

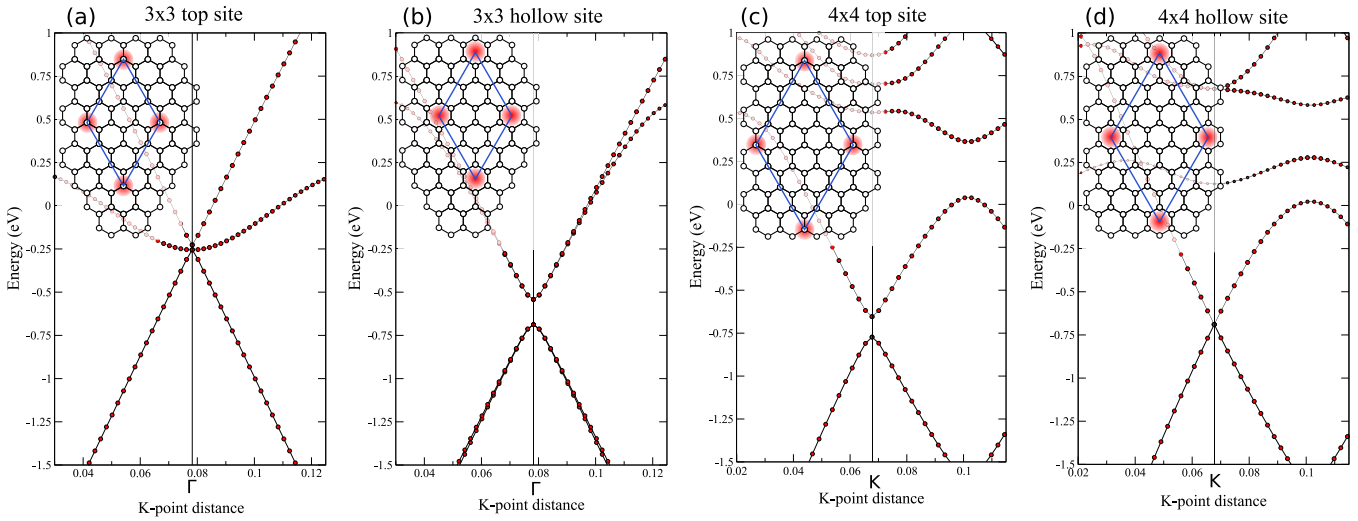

FIG. 6. DFT calculations of graphene band structure periodically perturbed by Si dangling bond located at different sites with respect to the graphene lattice. Hexagonal unit cell with periodicity multiple of $\sqrt{3}$ (including 3×3) cell results in semimetallic bands in the case of top site interaction and semiconducting bands with sizable band gap in the case of hollow site intercalation. The opposite is true for other periodicities (like 4×4) in this figure.

i.e., $(\sqrt{3} \times \sqrt{3})$R30°, (3×3), $(2\sqrt{3} \times 2\sqrt{3})$R30°, (6×6) and so on [Fig. 6(a)]. However, for other hexagonal graphene cells the band gap will open [Fig. 6(c)]. The situation is opposite when an Si dangling bond is located under the center of the C ring, i.e., for the hollow site [see example in Figs. 6(b) and 6(d)]. It has to be noted that hollow site configurations occur to be quite unstable, as the allowed structural relaxation results in significant graphene-substrate separation and decoupling of electronic structure. The on-top configuration on the contrary gives the strongest bonding between Si adatom and graphene. The energy difference between these two sites after relaxation is ∼0.5 eV. It will not be practical to use simplified reduced unit cell size, such as SiC(0001)-(3×3), with slightly stretched graphene (∼8.4% to match the cell) to model the SiC/interface/graphene structure, as the local defect sites would be completely different from the real case as well as unit cell size. One has to use at least a full $6\sqrt{3}$ cell which gives the smallest lattice mismatch between graphene and SiC, although decoupling of the graphene layer, disappearance of $6\sqrt{3}$ reflexes in LEED pattern, and slight disorder of bright features in the STM image may indicate relaxation of the graphene lattice to a completely incommensurate one. The fact that the actual unit cell is not actually (3×3) as appears in LEED, but much larger, is also evident from STM images, where large spatial variations were observed as bright "6×6" triangular-shaped protrusions. The $6\sqrt{3}$ SiC/interface/graphene system is, unfortunately, too large to be treated within the DFT approach. So, after performing tests on smaller units and making sure that two methods give similar results in terms of electronic structure, we used the self-consistent charge density functional theory tight-binding (SCC-DFTB) method within the DFTB+ package [42,43] for our calculations. In Figs. 7(a) and 7(b) the initial model is shown. Naturally, one may think to put the graphene layer so that one of the carbon atoms is directly on top of the Si adatom, as an on-top site allows one of the most stable bonding configurations. Due to the lattice mismatch, however, this implies the existence of Si adatoms also under one hollow site, three bridge sites, and six top shifted sites as shown in Fig. 7(b). The periodicity of local defects of various types in this model is strictly $6\sqrt{3}$ which is not in good agreement with STM quasi-"6×6" observations. If we, however, shift graphene's lattice just by $a_{Gr}/3$ along graphene's [1000] direction, the situation resolves as shown in Fig. 7(c). In this case we will have three types of Si adatom locations: six slightly misplaced top sites (the shift is much smaller than in previous model shifted sites), three shifted hollow sites, and three misplaced bridge sites. The local C-Si bonding configuration of the six misplaced top sites closely resembles simple on-top configuration with slight distortion. As the average number of these sites with possible direct Si-C bonds is increased, this may give more stability to the structure. Indeed, SCC-DFTB calculations show that the shifted model has lower, although marginally (by 2 meV), total energy compared to nonshifted. Additionally, if we neglect rotation of local structures of these defects (all rotational orientation will result in quite similarly looking LDOS distributions), these sites form (6×6) periodicity observed by STM. Although this is a rough estimation and it requires more justification, the model, however, is quite valid. The calculated band structure is shown in Fig. 7(d). The graphene layer appears to be decoupled from the surface with linear gapless dispersion near the Dirac point. The Dirac point is shifted by 0.26 eV below Fermi level as a result of n-type doping of the graphene layer by Si adatoms. The calculated dispersion is in good agreement with experimental data. Thus, we think that the proposed model may indeed represent the interface structure formed by Si in between graphene sheet and SiC surface.

The fact that graphene's band structure properties are so sensitive to location and periodicity of external influence, as well as the existence of a variety of interface structures and ease with which they could be created by simple intercalation of Si or other atoms, opens really attractive perspectives of manipulating graphene's properties by means of creating a

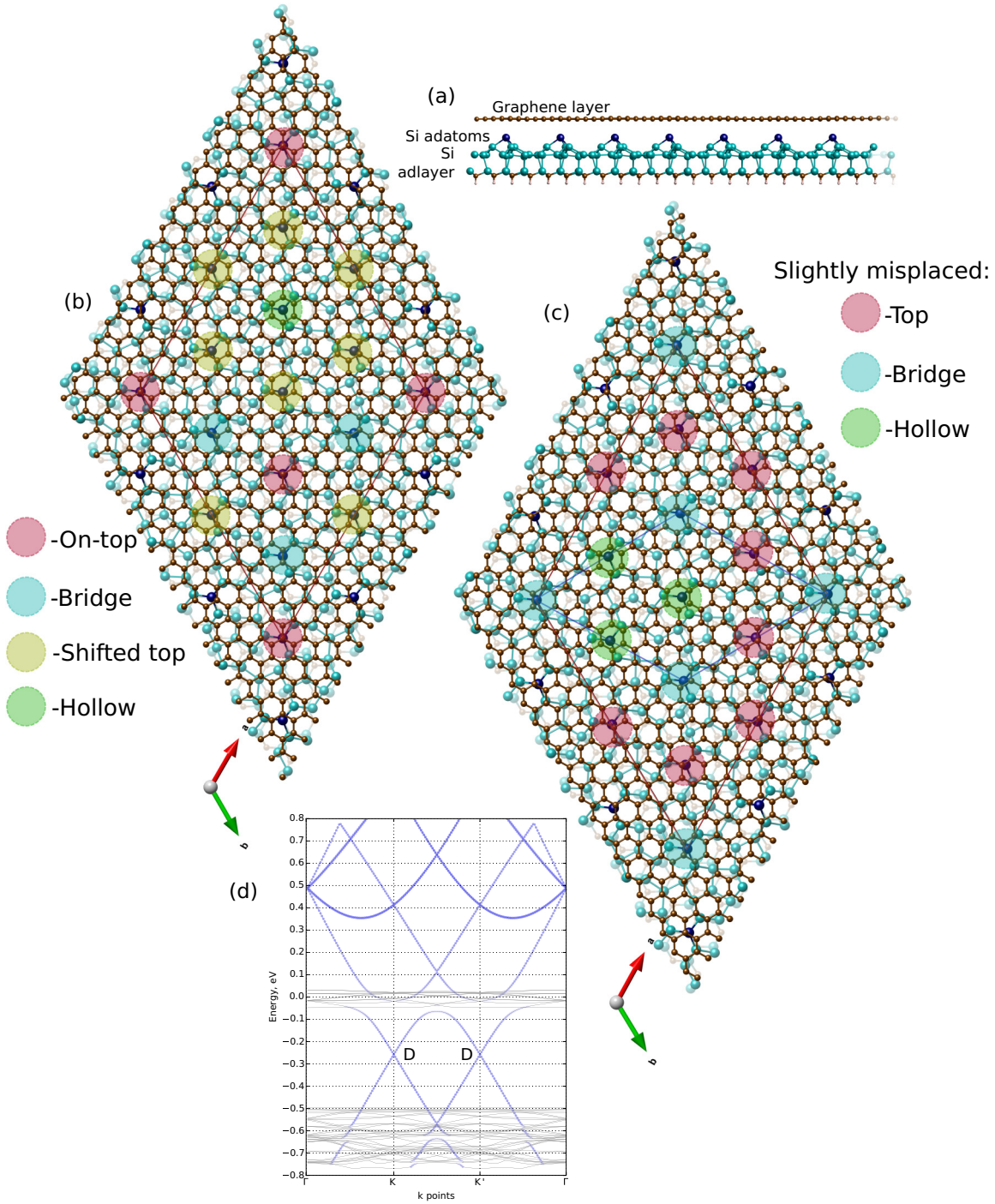

FIG. 7. (a) Side view of graphene/Si-(3×3)/SiC(0001) model. (b) Top view of the simple nonshifted model, one can see four different local interaction sites. All sites have $6\sqrt{3}$ period on the surface. (c) Top view of the model with slightly shifted graphene layer. There are three different local interaction sites with "shifted bridge site" having (6×6) arrangement (though rotated 120^o). (d) The band structure of the calculated model. Blue circles represent bands localized on the graphene layer as was determined by decomposition analysis. The "D" symbols denote positions of Dirac points.

right interface structure between graphene and the substrate. In the case of the (3×3)-Si interface graphene's unit cell is rather large (13×13) and includes several different interaction sites in a manner that on average the sublattice symmetry is maintained, which results in zero band gap. According to ARPES, the similar results are obtained for lower coverage hexagonal and rectangularlike interfaces. However, other interface structures are possible with other intercalants which may result in a semiconducting graphene layer.

IV. CONCLUSIONS

In conclusion, we have studied the interface structures formed by Si intercalation in the region between SiC surface

and graphene sheet by LEED, STM, and first principles calculations. We have shown that, by Si intercalation, the graphitic buffer layer is decoupled from the substrate and converted to a true graphene layer with linear electron dispersion in the vicinity of K and K' points of graphene's Brillouin zone. The interface structures formed by Si atoms vary depending on the amount of intercalated Si. The set of these structures mimics the same atomic arrangements formed by Si adsorption on the clean SiC(0001) surface as evident from strikingly similar STM appearance to previously reported data and from XPS analysis. SCC-DFTB full unit cell calculations support experimental results of decoupling of the graphene layer and restoring the Dirac cone with zero band gap and n-type doping. Using rather naive consideration we proposed the simple model of the graphene overlayer on top of the SiC(0001)-(3×3)-Si structure with slight lateral shift to explain the apparent (6×6) period in STM images. As was suggested previously and supported by our own calculations, the graphene electronic structure is very sensitive to the period of applied external potential and its localization. Such a wide variety of possible interface structures in terms of period and local atomic arrangement produced by intercalation of Si and other materials may open the way for electronic structure modification of graphene layers on substrates, particularly on SiC, which cannot be underestimated for practical device applications.

[1] L. Torres, S. Roche, and J. Charlier, *Introduction to Graphene-Based Nanomaterials: From Electronic Structure to Quantum Transport* (Cambridge University Press, New York, 2014).

[2] E. P. Randviir, D. A. Brownson, and C. E. Banks, Mater. Today **17**, 426 (2014).

[3] F. Schwierz, Nat. Nanotechnol. **5**, 487 (2010).

[4] K. S. Novoselov, V. I. Fal'ko, L. Colombo, P. R. Gellert, M. G. Schwab, and K. Kim, Nature (London) **490**, 192 (2012).

[5] K. V. Emtsev, A. Bostwick, K. Horn, J. Jobst, G. L. Kellogg, L. Ley, J. L. McChesney, T. Ohta, S. a. Reshanov, J. Röhrl, E. Rotenberg, A. K. Schmid, D. Waldmann, H. B. Weber, and T. Seyller, Nat. Mater. **8**, 203 (2009).

[6] K. V. Emtsev, F. Speck, T. Seyller, L. Ley, and J. D. Riley, Phys. Rev. B **77**, 155303 (2008).

[7] J. D. Emery, B. Detlefs, H. J. Karmel, L. O. Nyakiti, D. K. Gaskill, M. C. Hersam, J. Zegenhagen, and M. J. Bedzyk, Phys. Rev. Lett. **111**, 215501 (2013).

[8] L. H. de Lima, A. de Siervo, R. Landers, G. A. Viana, A. M. B. Goncalves, R. G. Lacerda, and P. Häberle, Phys. Rev. B **87**, 081403 (2013).

[9] F. Varchon, R. Feng, J. Hass, X. Li, B.N. Nguyen, C. Naud, P. Mallet, J.-Y. Veuillen, C. Berger, E.H. Conrad, and L. Magaud, Phys. Rev. Lett. **99**, 126805 (2007).

[10] E. Pallecchi, F. Lafont, V. Cavaliere, F. Schopfer, D. Mailly, W. Poirier, and A. Ouerghi, Sci. Rep. **4**, 4558 (2014).

[11] C. Riedl, C. Coletti, T. Iwasaki, A. A. Zakharov, and U. Starke, Phys. Rev. Lett. **103**, 246804 (2009).

[12] J. Sforzini, L. Nemec, T. Denig, B. Stadtmüller, T.-L. Lee, C. Kumpf, S. Soubatch, U. Starke, P. Rinke, V. Blum, F. C. Bocquet, and F. S. Tautz, Phys. Rev. Lett. **114**, 106804 (2015).

[13] F. Bisti, G. Profeta, H. Vita, M. Donarelli, F. Perrozzi, P. M. Sheverdyaeva, P. Moras, K. Horn, and L. Ottaviano, Phys. Rev. B **91**, 245411 (2015).

[14] B. Premlal, M. Cranney, F. Vonau, D. Aubel, D. Casterman, M. M. De Souza, and L. Simon, Appl. Phys. Lett. **94**, 263115 (2009).

[15] T. P. Kaloni, M. Upadhyay Kahaly, Y. C. Cheng, and U. Schwingenschlögl, EPL (Europhysics Lett.) **99**, 57002 (2012).

[16] K. V. Emtsev, A. A. Zakharov, C. Coletti, S. Forti, and U. Starke, Phys. Rev. B **84**, 125423 (2011).

[17] F. Wang, K. Shepperd, J. Hicks, M. S. Nevius, H. Tinkey, A. Tejeda, A. Taleb-Ibrahimi, F. Bertran, P. Le Fèvre, D. B. Torrance, P. N. First, W. A. de Heer, A. A. Zakharov, and E. H. Conrad, Phys. Rev. B **85**, 165449 (2012).

[18] C. Xia, S. Watcharinyanon, A. A. Zakharov, R. Yakimova, L. Hultman, L. I. Johansson, and C. Virojanadara, Phys. Rev. B **85**, 045418 (2012).

[19] S. Oida, J. B. Hannon, and R. M. Tromp, Appl. Phys. Lett. **104**, 161605 (2014).

[20] Y. Cui, J. Gao, L. Jin, J. Zhao, D. Tan, Q. Fu, and X. Bao, Nano Research **5**, 352 (2012).

[21] T. P. Kaloni, M. U. Kahaly, Y. C. Cheng, and U. Schwingenschlogl, J. Mater. Chem. **22**, 23340 (2012).

[22] M. Silly, M. D'Angelo, A. Besson, Y. Dappe, S. Kubsky, G. Li, F. Nicolas, D. Pierucci, and M. Thomasset, Carbon **76**, 27 (2014).

[23] C. Mathieu, B. Lalmi, T. O. Mentes, E. Pallecchi, A. Locatelli, S. Latil, R. Belkhou, and A. Ouerghi, Phys. Rev. B **86**, 035435 (2012).

[24] S. Oida, F. R. McFeely, J. B. Hannon, R. M. Tromp, M. Copel, Z. Chen, Y. Sun, D. B. Farmer, and J. Yurkas, Phys. Rev. B **82**, 041411 (2010).

[25] Y. C. Cheng, Z. Y. Zhu, and U. Schwingenschlögl, EPL (Europhysics Lett.) **101**, 27008 (2013).

[26] M. G. Silly, G. Li, and Y. J. Dappe, Surf. Interface Anal. **46**, 1273 (2014).

[27] K. Wakabayashi, K.-i. Sasaki, T. Nakanishi, and T. Enoki, Sci. Technol. Adv. Mat. **11**, 054504 (2010).

[28] T. Kajiwara, Y. Nakamori, A. Visikovskiy, T. Iimori, F. Komori, K. Nakatsuji, K. Mase, and S. Tanaka, Phys. Rev. B **87**, 121407 (2013).

[29] A. A. Avetisyan, B. Partoens, and F. M. Peeters, Phys. Rev. B **79**, 035421 (2009).

[30] M. Yankowitz, F. Wang, C. N. Lau, and B. J. LeRoy, Phys. Rev. B **87**, 165102 (2013).

[31] Z. H. Ni, T. Yu, Y. H. Lu, Y. Y. Wang, Y. P. Feng, and Z. X. Shen, ACS Nano **2**, 2301 (2008).

[32] M. S. Nevius, M. Conrad, F. Wang, A. Celis, M. N. Nair, A. Taleb-Ibrahimi, A. Tejeda, and E. H. Conrad, Phys. Rev. Lett. **115**, 136802 (2015).

[33] M. Dvorak and Z. Wu, Phys. Rev. B **90**, 115415 (2014).

[34] M. Dvorak and Z. Wu, Nanoscale **7**, 3645 (2015).

[35] S. Y. Zhou, G.-H. Gweon, A. V. Fedorov, P. N. First, W. A. de Heer, D.-H. Lee, F. Guinea, A. H. Castro Neto, and A. Lanzara, Nat. Mater. **6**, 916 (2007).

[36] L. Li, Y. Hasegawa, I. S. Tsong, and T. Sakurai, J. Phys. IV France **06**, C5-167 (1996).
[37] M. Naitoh, J. Takami, S. Nishigaki, and N. Toyama, Appl. Phys. Lett. **75**, 650 (1999).
[38] A. Fissel and J. Dąbrowski, Surf. Rev. Lett. **10**, 849 (2003).
[39] C. Riedl, C. Coletti, and U. Starke, J. Phys. D **43**, 374009 (2010).
[40] U. Starke, J. Bernhardt, J. Schardt, and K. Heinz, Surf. Rev. Lett. **06**, 1129 (1999).
[41] Y. Hoshino, T. Okawa, M. Shibuya, T. Nishimura, and Y. Kido, Surf. Sci. **602**, 3253 (2008).
[42] M. Elstner, D. Porezag, G. Jungnickel, J. Elsner, M. Haugk, T. Frauenheim, S. Suhai, and G. Seifert, Phys. Rev. B **58**, 7260 (1998).
[43] B. Aradi, B. Hourahine, and T. Frauenheim, J. Phys. Chem. A **111**, 5678 (2007).